Finite and infinite matrix product states for Gutzwiller projected mean-field wave functions

Gabriel Petrica,[1,*] Bo-Xiao Zheng,[2,3] Garnet Kin-Lic Chan,[2] and Bryan K. Clark[1,†]

[1]*Institute for Condensed Matter Theory and IQUIST and Department of Physics, University of Illinois at Urbana-Champaign, Urbana, Illinois 61801, USA*

[2]*Division of Chemistry and Chemical Engineering, California Institute of Technology, Pasadena, California 91125, USA*

[3]*AxiomQuant Investment Management LLC, Shanghai 200120, China*

(Received 18 January 2021; revised 15 March 2021; accepted 17 March 2021; published 31 March 2021)

Matrix product states (MPS) and "dressed" ground states of quadratic mean fields (e.g., Gutzwiller projected Slater determinants) are both important classes of variational wave functions. This latter class has played important roles in understanding superconductivity and quantum spin liquids. We present a method to obtain both the finite and infinite MPS (iMPS) representation of the ground state of an arbitrary fermionic quadratic mean-field Hamiltonian (which in the simplest case is a Slater determinant and in the most general case is a Pfaffian). We also show how to represent products of such states (e.g., determinants times Pfaffians). From this representation one can project to single occupancy and evaluate the entanglement spectra after Gutzwiller projection. We then obtain the MPS and iMPS representation of Gutzwiller projected mean-field states that arise from the variational slave-fermion approach to the $S = 1$ bilinear-biquadratic quantum spin chain. To accomplish this, we develop an approach to orthogonalize degenerate iMPS to find all the states in the degenerate ground-state manifold. We find the energies of the MPS and iMPS states match the variational energies closely, indicating the method is accurate and there is minimal loss due to truncation error. We then present an exploration of the entanglement spectra of projected slave-fermion states, exploring their qualitative features and finding good qualitative agreement with the respective exact ground-state spectra found from density matrix renormalization group.

DOI: 10.1103/PhysRevB.103.125161

I. INTRODUCTION

Variational wave functions are frequently used to understand quantum many-body systems. Two important classes of variational wave functions are dressed Slater determinants and tensor networks. Dressed Slater determinants introduce a correlation on top of a mean-field ground state. On the other hand, a tensor network is represented as a network of connected tensors providing a natural framework in which to understand and represent low-entangled quantum states (see Fig. 1).

Slater determinants (SDs) [and other generalized quadratic ground states such as Bogoliubov–de Gennes (BdG) [1] and Pfaffian states [2]] have played a key role in the understanding of physical systems ranging from their use as the Hartree-Fock solution in quantum chemistry to being applied as a starting mean-field *Ansatz* for strongly correlated systems. These latter *Ansatzë* are then dressed in various ways: Slater-Jastrow wave functions are the *de facto* standard for simulating material systems in quantum Monte Carlo; many prototypical quantum Hall states are represented as powers or products of Slater determinants and Pfaffians; and projected mean-field states are an important starting point for probing the physics of high-temperature superconductivity as well as quantum spin liquids.

While dressed mean-field states are often easy to represent in variational Monte Carlo (VMC), it is also often difficult to extract certain properties from VMC. Foremost among these are the entanglement spectra which are an important metric used for understanding topological phases of matter. Even properties which can be extracted easily, such as the energy, can be statistically noisy, making aspects such as optimization difficult. Moreover, evaluating dressed mean-field states in Monte Carlo scales cubically with the system size, making the approach to the thermodynamic limit costly. Matrix product states avoid many of these problems in one-dimensional systems and ladders: They are ideally suited for extracting entanglement spectra, computing observables exactly without any statistical noise, and directly representing (gapped) physical systems in the thermodynamic limit.

Our main contribution in this paper is to describe a series of efficient and highly parallel algorithms which take (projected) mean-field (i.e., quadratic) eigenstates and generate both finite (fMPS) and infinite (iMPS) matrix product states (MPS) from them. We will also show how to generate fMPS and iMPS for products of mean-field wave functions. We will then apply our approach to compute the MPS and entanglement spectra of a series of projected slave-fermion wave functions of the bilinear-biquadratic model. This example will bring to light a number of interesting aspects of generating multiple degenerate ground states from Gutzwiller projected slave-fermion systems in iMPS.

Beyond this particular application, being able to generate a MPS from a projected SD is generically useful. It allows for

*petrica2@illinois.edu
†bkclark@illinois.edu

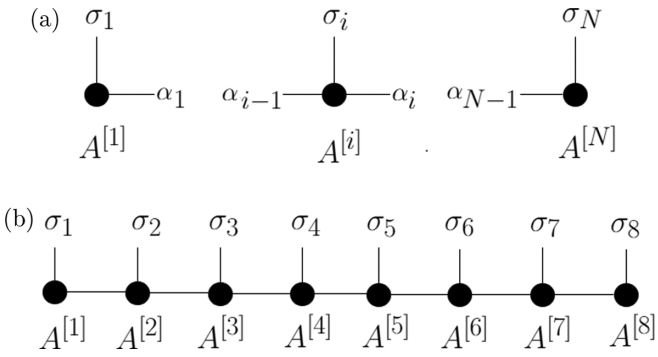

FIG. 1. (a) Graphical representation of the left-boundary, bulk, and right-boundary A tensors forming an open-boundary matrix product state. The α's are the virtual indices; the σ's are the physical indices. (b) Graphical representation of an eight-site matrix product state.

more faithful comparisons between slave-fermion and density matrix renormalization group (DMRG) results which often disagree on the underlying phase of spin liquids. It could be used to initialize DMRG with a good initial mean-field guess for certain Hamiltonians. This can be useful both for calculations on discrete lattices as well as DMRG in the continuum. Because there exist algorithms which build MPS on quantum computers, it immediately gives an additional approach to generate a dressed quadratic mean-field state on a quantum device.

We are aware of two other algorithms which convert Slater determinants to MPS [3–5]. Both of these are based on the idea of applying quantum gates or matrix product operators to a simpler quantum state to generate the MPS. Our approach differs from these techniques in two key ways: (1) We can generate the infinite MPS for a family of Slater determinants and (2) we generate our (i)MPS by directly generating the MPS coefficients without the application of any operators to the system. We also note that Ref. [6] represents Slater determinants in a MPS-like framework in a Gaussian fermionic representation.

In Sec. II, we will describe our key algorithm for turning a SD into an (i)MPS. In Sec. III, we will show a series of examples for how to use this basic procedure for generating more complicated mean-field states (i.e., Pfaffians) as well as states which are products of mean-field states. Finally, in Sec. IV we focus on computing (i)MPS for the slave-fermion states of the bilinear-biquadratic model showing their entanglement spectra and energy.

II. SLATER DETERMINANTS TO MPS

In this section we are going to show how to generate either a finite matrix product state (fMPStoSD) or an infinite matrix product state (iMPStoSD) from a Slater determinant (SD). This will not only be useful in its own right but will be the key operation used in the rest of this work to produce MPS for both more complicated quadratic mean-field states as well as dressed versions of these states.

The fMPStoSD generates the matrix product state site by site in an approach that is highly reminiscent of the site-decimation canonical technique to convert a generic wave function (i.e., a multisite tensor) into a matrix product state [7]. The typical site-decimation procedure involves performing singular value decompositions (SVDs) over matrices generated by collecting different subsets of indices into the two matrix dimensions. This general approach will become efficient to use with Slater determinants because SVDs of Slater determinants are efficient and generate sums of products of Slater determinants.

In fMPStoSD we perform a series of Schmidt decompositions over all bipartitions of our system. Each Schmidt decomposition generates a set of Schmidt vectors; each such Schmidt vector is a Slater determinant. The MPS is then generated by taking overlaps of these Slater determinant Schmidt vectors with each other in the correct way.

In iMPStoSD we can easily generate the bulk uniform iMPS tensor from *just* two Schmidt decompositions: one for each of two ground-state Slater determinants of the same Hamiltonian defined on sufficiently large systems that differ in size by one unit cell. Again, these Schmidt decompositions will have Slater determinant Schmidt eigenvectors. After we appropriately fix the gauge of the two Schmidt decompositions, the uniform bulk MPS tensor will be generated from appropriate overlaps of these Schmidt eigenvectors.

A. Slater determinant→finite MPS

In this section, we show in detail how to convert a Slater determinant into a finite matrix product state. The Schmidt decomposition of a Slater determinant $|\mathrm{SD}\rangle$ on N sites bipartitioned into two regions cut between sites i and $i+1$ will be notated as

$$|\mathrm{SD}\rangle = \sum_{\alpha} \lambda_{\alpha}^{i;N} \left|L_{\alpha}^{i;N}\right\rangle \left|R_{\alpha}^{i;N}\right\rangle, \tag{1}$$

where $|L_\alpha\rangle$ and $|R_\alpha\rangle$ are the αth left and right Schmidt vectors, respectively (with support in their respective subsystem), and λ_α is the αth Schmidt eigenvalue. Note that, for a Slater determinant, each of the individual left and right Schmidt vectors are also Slater determinants and efficiently computable [8–11] [see also Supplemental Material (SM) 3 [12] for more details regarding the Schmidt decomposition of Slater determinants]. Slater determinants are specified by a set of single-particle orbitals and all the Slater determinants in the set of right Schmidt vectors $\{|R_\alpha\rangle\}$ are specified by subsets of single-particle orbitals from a set of (at most) N single-particle orbitals $\{\phi_1^R \cdots \phi_N^R\}$ defined on the (inclusive) sites $[(i+1), \ldots, N]$. There are, at most, 2^N such subsets. Analogous statements hold for the left Schmidt vectors.

A general matrix product state can be written as

$$|\mathrm{MPS}\rangle = \sum_{\{\sigma\},\{a\}} A_{1,a_1}^{[1]\sigma_1} \cdots A_{a_{N-1},1}^{[N]\sigma_N} |\sigma_1 \cdots \sigma_N\rangle, \tag{2}$$

where $A^{[k]}$ is the kth three-tensor specified by the physical index σ_k (e.g., occupancy or spin) and the virtual indices (α_{k-1}, α_k) [7]. To generate the MPS of a Slater determinant, we compute each three-tensor $A^{[i+1]}$ as

$$A_{\alpha_k\alpha_{k+1}}^{[i+1]\sigma_{i+1}} = \left(\langle\sigma_{i+1}| \otimes \langle R_{\alpha_{k+1}}^{i+1;N}|\right) |R_{\alpha_k}^{i;N}\rangle, \tag{3}$$

giving a matrix which is in right canonical form, i.e., $\sum_\sigma A^{[i+1]\sigma}(A^{[i+1]\sigma})^\dagger = I$. Note that this procedure is very similar to the one which transforms a vector into a MPS [7] and works for the same reason: The sets $\{|R_\alpha^{i;N}\rangle\}$ and $\{|\sigma_i\rangle \otimes |R_\beta^{i+1;N}\rangle\}$ span the same space and therefore there is a transformation A which rotates between them. In practice, we keep the bond dimension of A controlled by only computing the Schmidt vectors whose Schmidt values are above a certain threshold ϵ. This can be done without computing any Schmidt eigenvector with an eigenvalue less than ϵ. Here, we have focused on the bulk tensors and slight modifications need to be made for the boundary tensors $A^{[1]\sigma_1}$ and $A^{[N]\sigma_N}$ (see SM 1 [12] for the mathematical expression of the boundary tensors). We now describe how to efficiently evaluate the matrix elements of each A. We start by noting that $|\sigma_{i+1}\rangle \otimes |R^{i+1;N}\rangle$ is also a Slater determinant. It is specified by the single-particle orbitals

$$\{[0\phi_a], [0\phi_b], \ldots, [0\phi_c], \phi^{i+1}\}, \tag{4}$$

where $[0\phi_a]$ is the single-particle orbital with coefficients in the lattice basis $[0, \phi_a(i+2), \phi_a(i+3), \ldots, \phi_a(N)]$ and ϕ^{i+1} is the single-particle orbital in analogous notation, $[1, 0, \ldots, 0]$. Equation (3) then reduces to the overlap of two Slater determinants of size $(N-i)\times(N-i)$ which can be computed in $O(N^3)$ time.

While naively each element of A requires such a computation, there is a significant overlap in these different computations which reduces the naive computational complexity of the tensor computation. There are two steps in computing the overlap of two Slater determinants: evaluating the overlap matrix between all pairs of single-particle orbitals that make up the two determinants and computing the determinant of this overlap matrix. All the Slater determinants used in the ket (respectively bra) of Eq. (3) (over different terms in A) come from a subset of single-particle orbitals of the N-orbital set $\{\phi_1^R, \ldots, \phi_N^R\}$. We can compute the overlap matrix of all these respective single-particle orbitals once per three-tensor A at a cost of $O(N^3)$. The entries of A are then determinants of submatrices of this overlap matrix. While naively each determinant also costs $O(N^3)$ to compute, the submatrices differ only in the bottom $\log_2 D$ columns and right $\log_2 D$ rows where D is the bond dimension of A; determinant update formulas can then be used to accelerate this computation, letting each determinant be computed in time $O(N^2 \log_2 D)$ after an initial $O(N^3)$ operation to evaluate the inverse of the upper-left $(N-\log_2 D)\times(N-\log_2 D)$ block of the overlap matrix. The whole evaluation of each tensor A can be done in $O(N^3)+O(D^2N^2\log_2 D)$ time. This can be further attenuated somewhat by more aggressive use of determinant update formulas [13].

Notice that there are significant parts of this algorithm that can be run in parallel. Each three-tensor A can be computed separately. Within each A, the Schmidt decomposition can be partially parallelized; each element of the overlap matrix can be computed in parallel; and, after the initial evaluation of the inverse of the upper-left block of the overlap matrix, each determinant can then be computed in parallel. See Fig. 2.

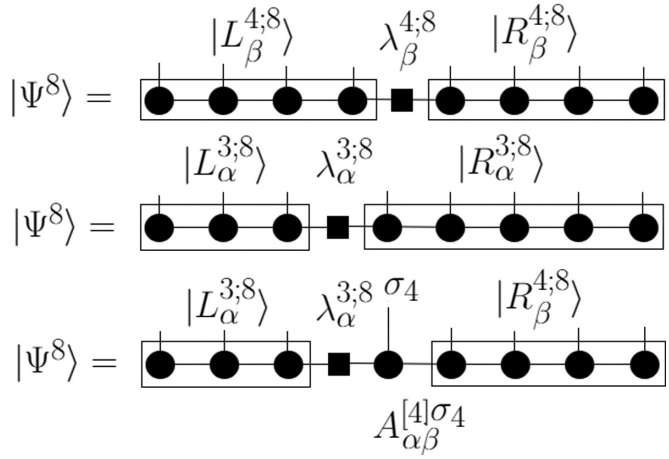

FIG. 2. Top: Graphical representation of the Schmidt decomposition of the wave function $|\Psi^8\rangle = \sum_\beta \lambda_\beta^{4;8} |L_\beta^{4;8}\rangle |R_\beta^{4;8}\rangle$ over a bipartition $[1,\ldots,4]\times[5,\ldots,8]$ of an eight-site system. Middle and bottom: Two additional ways of representing the quantum state $|\Psi_8\rangle$. The tensor $A^{[4]}$ is constructed by having the overlap of the right five sites of the bottom two figures equal one.

B. Gapped Slater determinant→infinite MPS

The above procedure generates a finite MPS approximation (the accuracy of the representation is given as an input to the algorithm) of any Slater determinant. In this section, we describe how to generate an infinite MPS from the Slater determinant ground state of a gapped mean-field Hamiltonian. This infinite MPS can be described by left L and right R boundary tensors which sandwich the bulk tensor A, giving us an infinite matrix product state of the form

$$|\text{iMPS}\rangle = \sum_\sigma L^{\sigma_L}\cdots A^{\sigma_{n-1}}A^{\sigma_n}A^{\sigma_{n+1}}\cdots R^{\sigma_R} \times |\sigma_L\cdots\sigma_{n-1}\sigma_n\sigma_{n+1}\cdots\sigma_R\rangle\,, \tag{5}$$

with an arbitrary number of bulk tensors A. L and R are tensors which span a fixed number k of sites. Note that any thermodynamic observable can be computed directly in the thermodynamic limit of the Slater determinant using only the bulk tensor A. In addition, we can compute the amplitude for the Slater determinant on any (large enough) system size, by inserting the corresponding number of bulk tensors between the boundary tensors L and R (i.e., to generate the MPS for an N-site Slater determinant from the infinite MPS, we therefore use $N-2k$ bulk tensors A); see Fig. 3.

To generate the iMPS, we start off by producing two Slater determinants defined on $2N$ and $2N+1$ sites (see Fig. 4), where N is sufficiently large such that the entanglement spec-

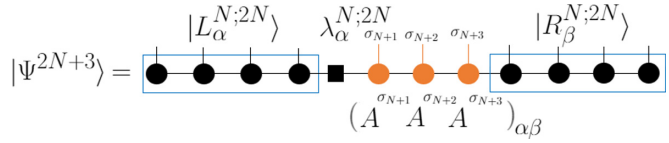

FIG. 3. We obtain the finite MPS $|\psi^{2N+n}\rangle$ by inserting n (in the figure $n=3$) A iMPS bulk tensors between the left $|L^{N/2;N}\rangle$ and right $|R^{N/2;N}\rangle$ Schmidt vectors obtained from $|\psi^{2N}\rangle$.

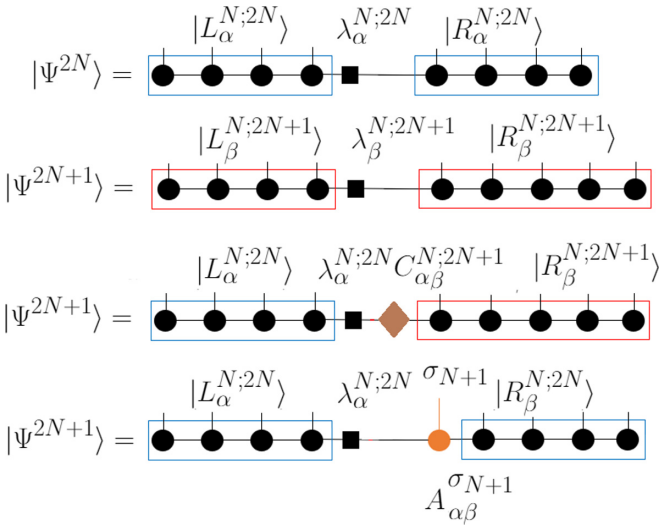

FIG. 4. Illustration of the algorithm for generating the infinite MPS representation of a Slater determinant. Lines 1 and 2 correspond to the standard Schmidt decomposition after site N of wave functions defined on $2N$ and $2N+1$ sites. For line 3, we use our gauge freedom to replace the left Schmidt eigenvalues $\lambda^{N;2N+1}$ and eigenvectors $|L^{N;2N+1}\rangle$ with eigenvalues $\lambda^{N;2N}$ and eigenvectors $|L^{N;2N}\rangle$ rotated by C where C is defined in Eq. (9). Finally, the tensor A is constructed by having the overlap of the right $N+1$ sites (including C) of the bottom two lines equal one.

trum is constant over cuts in the "bulk" of the wave functions. For gapped systems, we generically expect the entanglement spectrum over the bulk to be constant; see Fig. S3 in SM 5 [12] for an example of this and for entanglement spectrum data in the context of the Su-Schrieffer-Heeger (SSH) model. We then generate the Schmidt decompositions

$$|\Psi^{2N}\rangle = \sum_{\alpha} \lambda_{\alpha}^{N;2N} |L_{\alpha}^{N;2N}\rangle |R_{\alpha}^{N;2N}\rangle, \tag{6}$$

$$|\Psi^{2N+1}\rangle = \sum_{\alpha} \lambda_{\alpha}^{N;2N+1} |L_{\alpha}^{N;2N+1}\rangle |R_{\alpha}^{N;2N+1}\rangle. \tag{7}$$

Both $|L_{\alpha}^{N;2N}\rangle$ and $|L_{\alpha}^{N;2N+1}\rangle$ are going to be the same up to a gauge freedom. We fix this gauge freedom by defining a unitary

$$\begin{aligned} C_{\alpha\beta}^{N;2N+1} &= 0 \quad \text{if } \lambda_{\alpha} \neq \lambda_{\beta} \\ &= \langle L^{N;2N}|_{\alpha} \, |L^{N;2N+1}\rangle_{\beta} \quad \text{otherwise,} \end{aligned} \tag{8}$$

which rotates between Schmidt eigenvectors with the same Schmidt eigenvalue allowing the state on $2N+1$ sites to be defined as

$$|\Psi^{2N+1}\rangle = \sum_{\alpha\gamma} |L^{N;2N}\rangle_{\alpha} \, \lambda_{\alpha}^{N;2N+1} C_{\alpha\gamma}^{N;2N+1} \, |R^{N;2N+1}\rangle_{\gamma} \, . \tag{9}$$

Then the tensor A for the iMPS is

$$A_{\alpha\beta}^{\sigma_{N+1}} = \sum_{\gamma} C_{\alpha\gamma}^{[2N+1]} \, \langle \sigma_{N+1}| \, \langle R^{N;2N}|_{\beta} | \, |R^{N,2N+1}\rangle_{\gamma} \, . \tag{10}$$

As in the finite MPS case, we have that the single-particle orbitals of the Slater determinant $|\sigma_{N+1}\rangle|R^{N;2N}\rangle$ are shifted to the right with an initial zero as their first element. The overlap of this tensor can be computed in exactly the same way as for the finite MPS case. Here, though, we only need to evaluate one tensor A instead of a tensor per site, with the assumption that we are using an iMPS defined by a single tensor (i.e., single-site unit cell) A. This process can be generalized to multisite unit cells as well (see SM 2 [12] for the mathematical derivation). Note that by directly applying the finite MPS algorithm to large systems to try to find the bulk tensor A will fail because the gauge freedom available in the tensors will prevent a single identical bulk tensor from being produced at each step.

C. Numerical validation

We numerically validate our algorithms by applying fMPStoSD and iMPStoSD on the ground state of the Su-Schrieffer-Heeger (SSH) model [14],

$$\begin{aligned} H_{\text{SSH}} = v \sum_{n} (c_{n,1}^{\dagger} c_{n,2} + \text{H.c.}) \\ + w \sum_{n} (c_{n+1,1}^{\dagger} c_{n,2} + \text{H.c.}). \end{aligned} \tag{11}$$

The model describes spinless fermions on a one-dimensional (1D) lattice, with a two-site unit cell made up of A, B sites, with different (real) parameters for intracell hopping (v) and intercell hopping (w). It admits two different quantum ground states, distinct in their topological properties: a trivially gapped phase for $v > w$ and a (symmetry-protected) topological gapped ground state, characterized by the presence of two zero-energy edge modes inside the gap, for $v < w$, separated by a quantum critical point at $v = w$.

We will discuss here the trivial ground state. A small subtlety related to choosing the same gapless boundary mode in the Slater determinant wave functions used for generating the uniform tensor in the iMPS procedure is delegated to SM 4 [12] (where we show how we deal with gapless boundary modes in the context of the iMPS procedure). For the finite Slater determinant, we compare the MPS we generate using two different truncation values against the exact Slater determinant by comparing all of the amplitudes (see the first column in Fig. 5). For the infinite case, we generate the iMPS and then use the bulk tensor we have computed along with the boundary tensors to compute amplitudes for a much larger system and again compare amplitudes against the exact solution for that much larger system (see the second column in Fig. 5). In both cases, we find that the amplitudes are in very good agreement for all amplitudes down to the Schmidt eigenvalue cutoff.

III. GENERAL (DRESSED) QUADRATIC MEAN FIELDS

In Sec. II we showed how to generate a matrix product state from a Slater determinant. In this section, we show that this machinery gives us the means to generate the matrix product state representations of ground states of arbitrary quadratic mean-field Hamiltonians.

All quadratic Hamiltonians can be easily diagonalized using a canonical transformation [15]. Without loss of generality, in our derivations, we will use translation invariant systems for ease of presentation. We will first go through two canonical examples. In Sec. III A we will show how to

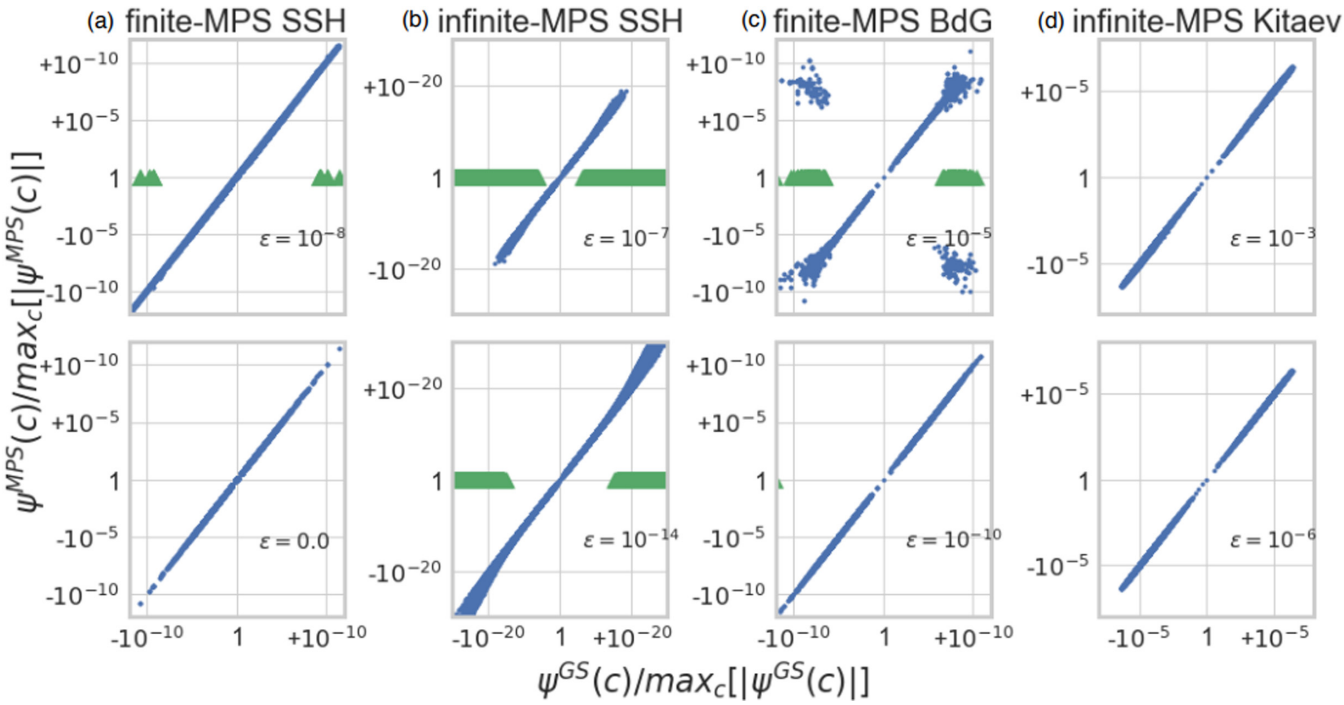

FIG. 5. Comparison of amplitudes (normalized by the largest amplitude seen) between our fMPS/iMPS wave functions and the exact SD. The largest (normalized) amplitude is at the "origin" of the graphs with smaller amplitudes toward both edges. Orange triangles are values at which the fMPS/iMPS gives zero amplitude; for these the "y" coordinate is arbitrarily set to 1. The amplitudes for the top row are less accurate as they are generated with larger MPS thresholds ϵ. (a) and (c) compare all amplitudes for $N = 8$ on [$v = 1.0$; $w = 0.6$; Eq. (11)] and [$t = 1$; $\mu = 3$; $\Delta = 1$; Eq. (16)], respectively. (b) We compare 459 428 random configurations (top and bottom are different configurations) between the $N = 24$ Slater determinant with ($v = 1.0$; $w = 0.6$) of Eq. (11) and a MPS generated from eight uniform iMPS bulk tensors (generated from SD on $N = 16, 17$ sites) sandwiched between the eight left and eight right tensors from the 16-site Slater determinant. (d) We compare 49 972 (top) and 34 933 (bottom) random configuration between the $N = 32$ Pfaffian ground state of the Kitaev chain with ($t = 1.0$; $\Delta = -1$ $\mu = -2.2$) of Eq. (17) and a MPS generated from eight uniform iMPS bulk tensors (generated from SD on $N = 24, 25$ sites) sandwiched between the 12 left and 12 right tensors from the 24-site Pfaffian.

produce the MPS representation of the ground states of BdG Hamiltonians which are Slater determinants in disguise. In Sec. III B, we show how to compute the MPS representation of the p-wave pairing ground state of the Kitaev chain [16]. We then generalize this result to general Pfaffian wave functions which are the most general quadratic mean-field ground states. Finally, we show how to take products (or powers) of quadratic mean-field Hamiltonians and turn them into (i)MPS.

A. BdG→MPS

The key trick to convert a BdG wave function into a MPS will be to (1) convert it to a Slater determinant through a particle-hole transformation, (2) convert this Slater determinant to a MPS, and (3) then undo the particle-hole transformation in the MPS language.

Consider a BdG Hamiltonian,

$$H_{\mathrm{BdG}} = -\sum_{\langle ij\rangle,\sigma} t_{ij}(c^\dagger_{i\sigma}c_{j\sigma} + \mathrm{H.c.}) - \sum_{\langle ij\rangle} \Delta_{ij}(c^\dagger_{i\uparrow}c^\dagger_{j\downarrow} + \mathrm{H.c.}) - \mu\sum_{i\sigma} c^\dagger_{i\sigma}c_{i\sigma}. \quad (12)$$

Under a canonical particle-hole transformation in the $\downarrow$ sector,

$$f^\dagger_{2i-1} = c^\dagger_{i\uparrow}, \qquad f^\dagger_{2i} = c_{i\downarrow}, \quad (13)$$

the BdG Hamiltonian becomes

$$H^{ph}_{\mathrm{BdG}} = -\sum_{\langle ij\rangle} t_{ij}(f^\dagger_{2i-1}f_{2j-1} - f^\dagger_{2i}f_{2j} + \mathrm{H.c.}) - \sum_{\langle ij\rangle} \Delta_{ij}(f^\dagger_{2i-1}f_{2j} + \mathrm{H.c.}) - \mu\sum_{i\sigma}(f^\dagger_{2i-1}f_{2i-1} - f^\dagger_{2i}f_{2i}), \quad (14)$$

and the new vacuum is $|0^{\mathrm{ph}}\rangle = c^\dagger_{1\downarrow}c^\dagger_{2\downarrow}\cdots c^\dagger_{N\downarrow}|0\rangle$, where $|0\rangle$ is the vacuum of the original theory. The ground state of H_{BdG} is thus the Slater determinant ground state of $H^{\mathrm{ph}}_{\mathrm{BdG}}$ on top of the new vacuum $|0^{\mathrm{ph}}\rangle$.

Using the results from Sec. II, we convert the Slater determinant ground state of $H^{\mathrm{ph}}_{\mathrm{BdG}}$ into a MPS $|\Psi_{\mathrm{MPS}}\rangle = \sum_{\{\sigma\}} A^{[1]\sigma_1}\cdots A^{[2N]\sigma_{2N}}|\sigma_1\cdots\sigma_{2N}\rangle$ where $\sigma_{2i-1} = \{0, 1\}$ ($i \in [1, N]$) indicates the absence/presence of a $\uparrow$ particle and $\sigma_{2i} = \{0, 1\}$ indicates the absence/presence of a *hole* on top of the filled $\downarrow$ Fermi sea at site i.

To "undo" the particle-hole transformation, we need to deal with the fact that the f_i act on the false vacuum $|0^{ph}\rangle$ (and not the real vacuum) by swapping, for all i, the matrices $A^{[2i]1}$ and $A^{[2i]0}$. Moreover, by ordering the fermionic operators by site, and then spin, the matrices $A^{[2i-1]1}, A^{[2i]1}$ will pick up factors of $(-1)^{i-1}$. We can now combine these transformations giving us our final MPS for the BdG ground state of the form $|\Phi_{\rm GS}\rangle = \sum_{\{\sigma=0,\uparrow,\downarrow,\uparrow\downarrow\}} B^{[1]\sigma_1}\cdots B^{[N]\sigma_N}|\sigma_1\cdots\sigma_N\rangle$ where

$$\begin{aligned} B^{[i]0} &= (-1)^{i-1}\times A^{[2i-1]0}A^{[2i]1},\\ B^{[i]\uparrow} &= (-1)^{2i-2}\times A^{[2i-1]1}A^{[2i]1},\\ B^{[i]\downarrow} &= (-1)^{0}\times A^{[2i-1]0}A^{[2i]0},\\ B^{[i]\uparrow\downarrow} &= (-1)^{i-1}\times A^{[2i-1]1}A^{[2i]0}. \end{aligned} \tag{15}$$

This approach works both for the finite and infinite MPS as we just used our (i)MPS→Slater determinant approach as a subroutine. For the infinite MPS it produces a unit cell of size 2 as every other B differs by a sign.

As a check of our algorithm, we consider the ground state of the BdG Hamiltonian of the form

$$\begin{aligned} H_{\rm BdG} = &-\sum_{\langle ij\rangle,\sigma} t_{ij}(c^\dagger_{i\sigma}c_{j\sigma}+{\rm H.c.})\\ &-\sum_{\langle ij\rangle}\Delta_{ij}(c^\dagger_{i\uparrow}c^\dagger_{j\downarrow}+c^\dagger_{j\uparrow}c^\dagger_{i\downarrow}+{\rm H.c.})-\mu\sum_{i\sigma}c^\dagger_{i\sigma}c_{i\sigma}, \end{aligned} \tag{16}$$

and compare the amplitudes of the exact ground state with the MPS generated (see the third column in Fig. 5).

B. Pfaffian→MPS

We will show how to generate a MPS representation of the Pfaffian ground state of the Kitaev p-wave chain:

$$\begin{aligned} H_c = &-t\sum_n(c^\dagger_n c_{n+1}+{\rm H.c.})+\Delta\sum_n(c^\dagger_n c^\dagger_{n+1}+{\rm H.c.})\\ &+\mu\sum_n c^\dagger_n c_n. \end{aligned} \tag{17}$$

We first consider $H^{\rm ext} = H_c \bigoplus H_d$ whose ground state is given by the tensor product of two identical Pfaffians,

$$|{\rm GS}\rangle = \sum_{\sigma_c,\sigma_d}{\rm Pf}(M_{\sigma_c})\,|\sigma_c\rangle\bigotimes Pf(M_{\sigma_d})\,|\sigma_d\rangle\,, \tag{18}$$

where M is an $N\times N$ matrix built from parameters of the model and M_{σ_c} is a submatrix of M obtained by selecting indices as given by the σ_c configuration.

Using the local canonical transformation of fermions,

$$\begin{aligned} c^\dagger_n &= \frac{(\bar c^\dagger_{n,\uparrow}+\bar c^\dagger_{n,\downarrow})}{\sqrt{2}},\\ d^\dagger_n &= i\frac{(\bar c^\dagger_{n,\uparrow}-\bar c^\dagger_{n,\downarrow})}{\sqrt{2}}, \end{aligned} \tag{19}$$

converts $H^{\rm ext}$ to

$$\begin{aligned} H_{\rm BdG} = &-t\sum_{n,\sigma}(\bar c^\dagger_{n,\sigma}\bar c_{n+1,\sigma}+{\rm H.c.})\\ &+\Delta\sum_n(\bar c^\dagger_{n\uparrow}\bar c^\dagger_{n+1\downarrow}+\bar c^\dagger_{n+1,\downarrow}\bar c^\dagger_{n,\uparrow}+{\rm H.c.})\\ &+\mu\sum_{n\sigma}\bar c^\dagger_{n,\sigma}\bar c_{n,\sigma}. \end{aligned} \tag{20}$$

The transformation leaves the vacuum unchanged. Given a BdG Hamiltonian, we can obtain the ground state as a MPS as done in Sec. III A,

$$|{\rm GS}\rangle = \sum_\sigma\cdots A^{[2i-1]\sigma_{2i-1}}A^{[2i]\sigma_{2i}}\cdots|\sigma_1\sigma_2\cdots\sigma_{2N}\rangle\,, \tag{21}$$

where $A^{[2i-1]\sigma_{2i-1}}$ is the tensor on site i for the $\uparrow$ local physical sector and $A^{[2i]\sigma_{2i}}$ is the tensor on site i for the $\downarrow$ local physical sector.

Notice that the canonical transformation given in Eq. (19) mixes the $\uparrow,\downarrow$ physical sectors on site i. Hence we can obtain the MPS for the GS in the c,d space by choosing the on-site tensor in the following way,

$$|{\rm GS}\rangle = \sum_\sigma C^{[1]\sigma_1}C^{[2]\sigma_2}\cdots C^{[N]\sigma_N}\,|\sigma_1\sigma_2\cdots\sigma_N\rangle\,, \tag{22}$$

with $\sigma=\{0,c,d,cd\}$ where

$$\begin{aligned} C^{[n],0} &= A^{[2n-1],0}A^{[2n],0},\\ C^{[n],c} &= \frac{A^{[2n-1],1}A^{[2n],0}+A^{[2n-1],1}A^{[2n],0}}{\sqrt{2}},\\ C^{[n],d} &= i\frac{A^{[2n-1],1}A^{[2n],0}-A^{[2n-1],1}A^{[2n],0}}{\sqrt{2}},\\ C^{[n],cd} &= iA^{[2n-1],1}A^{[2n],1}. \end{aligned} \tag{23}$$

By projecting out the d particles in the $|{\rm GS}\rangle$ wave function, we obtain a Pfaffian wave function in the c-particle sector: $|{\rm GS}\rangle = {\rm const}\times\sum_{\sigma_c}{\rm Pf}(M_{\sigma_c})\,|\sigma_c\rangle$. At the level of the MPS this projection is realized by eliminating the sectors $\sigma=\{d,cd\}$,

$$|{\rm Pf}\rangle = \sum_{\sigma=\{0,c\}} C^{[1]\sigma_1}C^{[2]\sigma_2}\cdots C^{[N]\sigma_N}\,|\sigma_1\sigma_2\cdots\sigma_N\rangle\,. \tag{24}$$

C. Pfaffian→MPS generalization

While we focused in the previous section on a specific example, here we consider a generic quadratic Hamiltonian $H=\sum_{n,m}C^\dagger_n h_{n,m}C_m$ with g species of fermions per unit cell where the vector $C^\dagger_n = (c^\dagger_{n,1}, c_{n,1}, c^\dagger_{n,2}, c_{n,2},\ldots, c^\dagger_{n,g}, c_{n,g})$.

We form an extended Hamiltonian $H^{\rm ext}$ which is a sum of two copies of H,

$$\begin{aligned} H^{\rm ext} = &\sum h^{\rm hop}_{i\alpha,j\beta}(c^\dagger_{i,\alpha}c_{j,\beta}+d^\dagger_{i,\alpha}d_{j,\beta}+{\rm H.c.})\\ &+\sum h^{\rm pair}_{i\alpha,j\beta}(c^\dagger_{i,\alpha}c^\dagger_{j,\beta}+d^\dagger_{i,\alpha}d^\dagger_{j,\beta}+{\rm H.c.}), \end{aligned} \tag{25}$$

where $\alpha,\beta\in(1,\ldots,g)$. As before, its ground state $|{\rm GS}\rangle^{\rm ext} = \sum_{\sigma_c,\sigma_d}{\rm Pf}(M_{\sigma_c})\,|\sigma_c\rangle\bigotimes{\rm Pf}(M_{\sigma_d})\,|\sigma_d\rangle$ is a tensor product of two identical Pfaffian wave functions. We then obtain the Pfaffian

ground state of H by projecting out all the d sectors. Under the following linear canonical transformation

$$\bar{c}^\dagger_{n,\alpha,\uparrow} = \frac{c^\dagger_{n,\alpha} + i d^\dagger_{n,\alpha}}{\sqrt{2}}, \qquad \bar{c}^\dagger_{n,\alpha,\downarrow} = \frac{c^\dagger_{n,\alpha} - i d^\dagger_{n,\alpha}}{\sqrt{2}}, \tag{26}$$

H^{ext} becomes a BdG-like Hamiltonian when expressed in terms of $c_\uparrow$ and $c_\downarrow$:

$$H^{\text{ext}}_{\text{BdG}} = \sum h^{\text{hop}}_{i\alpha,j\beta}(\bar{c}^\dagger_{i,\alpha,\uparrow}\bar{c}_{j,\beta,\uparrow} + \bar{c}^\dagger_{i,\alpha,\downarrow}\bar{c}_{j,\beta,\downarrow} + \text{H.c.}) + \sum h^{\text{pair}}_{i\alpha,j\beta}(\bar{c}^\dagger_{i,\alpha,\uparrow}\bar{c}^\dagger_{j,\beta,\downarrow} + \bar{c}^\dagger_{i,\alpha,\downarrow}\bar{c}^\dagger_{j,\beta,\uparrow} + \text{H.c.}). \tag{27}$$

We can then solve for the MPS representation of the ground state of the above BdG-like Hamiltonian using the methods described in Sec. III A.

We obtain the Slater determinant ground state $|\Psi_{\text{ext}}\rangle$ by diagonalizing the particle-hole transformed $H^{\text{ext}}_{\text{BdG}}$ and then computing its MPS representation. Each unit cell M is described by $2g$ tensors $A^{[M,p]\sigma}$ with $\sigma = 0, 1$ signifying the absence/presence of a particle of type $p \in [0, 1, \ldots, 2g-1]$. A particle of type $p = 2k$ corresponds to the flavor $k, \uparrow$; a particle of type $p = 2k+1$ corresponds to the flavor $k, \downarrow$. From the above MPS (which is in $\bar{c}_\uparrow, \bar{c}_\downarrow$ local physical space) we construct the MPS tensors in c, d space. In particular, the matrices describing the absence/presence of a particle of type c_i on site M are given by

$$B^{[M,i]0} = A^{[M,2i-1][0]}A^{[M,2i][1]}, \qquad B^{[M,i]1} = \frac{(-1)^{g(M-1)+i-1}}{\sqrt{2}} \times [A^{[M,2i-1][1]}A^{[M,2i][1]} + A^{[M,2i-1]0}A^{[M,2i][0]}], \tag{28}$$

where $(-1)^{g(M-1)+i-1}$ takes care of fermionic ordering. and the MPS representation of $|\Psi_{\text{GS}}\rangle$ defined on Ng sites is given by

$$|\Psi_{\text{GS}}\rangle = \sum_{\{\sigma\}} \left(B^{[1,1]\sigma_{1_1}} B^{[1,2]\sigma_{1_2}} \cdots B^{[1,g]\sigma_{1_g}}\right) \cdots \times \left(B^{[N,1]\sigma_{N_1}} B^{[N,2]\sigma_{N_2}} \cdots B^{[N,g]\sigma_{N_g}}\right) \times |\left(\sigma_{1_1}\sigma_{1_2}\cdots\sigma_{1_g}\right)\cdots\left(\sigma_{N_1}\sigma_{N_2}\cdots\sigma_{N_g}\right)\rangle. \tag{29}$$

By suitably contracting tensors we can obtain an N-tensor MPS representation with a physical dimension 2^g: $|\text{Pf}\rangle = \sum_\sigma C^{1\sigma_1}C^{2\sigma_2}\cdots C^{N\sigma_N}|\sigma_1\sigma_2\cdots\sigma_N\rangle$. For instance, the tensor corresponding to the *presence* of particles of type $t_1, t_2, \cdots, t_s$ on site M is

$$C^{[M](t_1,t_2,\ldots,t_s)} = B^{[M,1][0]}\cdots \times B^{[M,t_1][1]}B^{[M,t_1+1][0]}\cdots B^{[M,t_s][1]}\cdots B^{[M,g][0]}. \tag{30}$$

D. Power of Slater determinants

In this section we describe how to obtain the MPS representation of a wave function

$$|\psi_{1/n}\rangle = \sum_{r_1,r_2,\ldots,r_n} \langle r_1, r_2, \ldots, r_n|\psi\rangle^n |r_1, r_2, \ldots, r_n\rangle, \tag{31}$$

where $|\psi\rangle$ is a Slater determinant. We will use as an example $n = 3$. Products of other mean-field wave functions can be obtained similarly.

We extend our N-site system to a $3N$-site system for which we label the sites as $\{1_1 1_2 1_3 2_1 2_2 2_3 \cdots N_1 N_2 N_3\}$. We then write a single Slater determinant (by padding and interlacing the orbitals to keep the above ordering) of the form $|\psi\rangle \bigotimes |\psi\rangle \bigotimes |\psi\rangle$ for which we then convert into a MPS given by

$$|\text{MPS}\rangle = \sum_{i_p} (B^{[1_1]i_{1_1}} B^{[1_2]i_{1_2}} B^{[1_3]i_{1_3}}) \cdots \times (B^{[N_1]i_{N_1}} B^{[N_2]i_{N_2}} B^{[N_3]i_{N_3}}) \times |i_{1_1} i_{1_2} i_{1_3} \cdots i_{N_1} i_{N_2} i_{N_3}\rangle. \tag{32}$$

Projecting on the sector $i_{n_1} = i_{n_2} = i_{n_3}$ gives us the desired results of

$$|\psi_{1/3}\rangle = A^{[1]i_1}A^{[2]i_2}\cdots A^{[N]i_N}|i_1 i_2 \cdots i_N\rangle, \tag{33}$$

where we define

$$A^{[n]i_n} = B^{[n_1]i_{n_1}} B^{[n_2]i_{n_2}} B^{[n_3]i_{n_3}}. \tag{34}$$

IV. BILINEAR-BIQUADRATIC $S = 1$ MODEL

In this section, we use our approach to compute the MPS representation and entanglement spectra of the Gutzwiller projected slave-fermion mean-field states [17] of the bilinear-biquadratic (BLBQ) $S = 1$ model,

$$H = \sqrt{J_1^2 + J_2^2} \sum_{\langle i,j\rangle} [\cos\theta \mathbf{S}_i \cdot \mathbf{S}_j + \sin\theta (\mathbf{S}_i \cdot \mathbf{S}_j)^2], \tag{35}$$

The physics of the 1D quantum Heisenberg spin chain is qualitatively different for different spin representations [18]; half-integer spins have a gapless ground state and power-law spin correlations; integer spins have a gapped ground state with exponentially decaying correlations, the Haldane/Affleck-Kennedy-Lieb-Tasaki (AKLT) phase [19]. This latter phase is robust due to a combination of symmetries which protect its topological properties [20,21]. This symmetry protection can be understood in terms of "fractionalization": A $S = 1$ spin effectively splits into two $S = 1/2$ edge modes that transform under nontrivial projective representations of the symmetries (the product of the symmetry representations differs from the representation of the product). These features are reflected by nontrivial degeneracies in the entanglement spectrum [22,23], i.e., the eigenvalues of H_{ent} in $\rho_A = e^{-H_{\text{ent}}}$ where $\rho_A = \text{Tr}_B |\psi\rangle\langle\psi|$ is the reduced density matrix on an A subsystem [24–26]. The BLBQ model has four phases as shown in Fig. 6. This includes the Haldane phase (at the Heisenberg point), as well as a dimerized and critical phase.

One can derive the relevant projected mean-field state from the slave-fermion construction by fractionalizing the spin operators $\hat{\mathbf{S}}$ in terms of fermionic parton operators,

$$\hat{\mathbf{S}}_i = f^\dagger_{i;\alpha}\mathbf{S}_{\alpha\beta}f_{i;\beta}, \tag{36}$$

where $f^\dagger_{i;\alpha}$ is the α-flavor fermionic parton creation operator at site i and $\mathbf{S}_{\alpha\beta}$ are the matrix elements of the spin operators

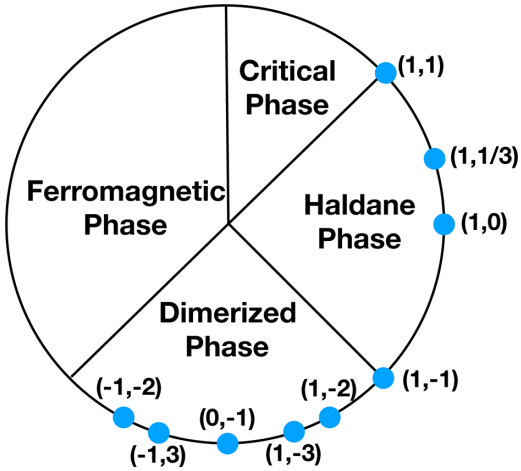

FIG. 6. Phase diagram of the bilinear-biquadratic $S = 1$ model. Figure reproduced from Ref. [17].

in a given representation S [27]. Substituting these expressions into the original Hamiltonian gives a quartic fermionic Hamiltonian H_f which can be decoupled through a mean field. The resulting mean-field ground state must then be projected back into the original Hilbert space, essentially "gluing" together the fractionalized degrees of freedom.

The slave-fermion construction of the bilinear-biquadratic model was studied in Ref. [17] where the authors used VMC to optimize the (χ, δ, μ) parameters of the projected wave function and studied the energy of this slave-fermion state compared to the exact energy achieved by the time-evolving block decimation (TEBD) algorithm. In this section, we will take the same points as studied in ref. [17,28], convert the slave-fermion states to MPS, and compute the entanglement spectra and the energies.

At the level of the Gutzwiller projected ground states, the two gapped phases, the dimer phase and the AKLT phase, are distinguished by their "fingerprint" in the low-lying structure of the entanglement spectrum: The lowest level of the entanglement spectrum of the dimerized topologically trivial phase is singly degenerate (for between dimer cuts); the lowest level of the entanglement spectrum of the Haldane phase ground state is doubly degenerate, corresponding to the presence of two boundary $S = 1/2$ edge modes.

A. Generating the MPS

The relevant mean-field Hamiltonian that arises from the parton construction of the bilinear-biquadratic $S = 1$ model [27,28] is

$$\begin{aligned} H_{\mathrm{mf}} = &-J\chi \sum_{i,\alpha=-1,0,1} [c^\dagger_{i,\alpha} c_{i,\alpha} + \mathrm{H.c.}] \\ &+ (J-K)\Delta \sum_{i,j} [c^\dagger_{i,-1} c^\dagger_{j,1} - c^\dagger_{0i} c^\dagger_{0j} + c^\dagger_{1i} c^\dagger_{-1j} + \mathrm{H.c.}] \\ &+ \lambda \sum_{i,\alpha} c^\dagger_{i\alpha} c_{i\alpha}, \end{aligned} \tag{37}$$

where the $c^\dagger_{-1}$, $c^\dagger_0$, and $c^\dagger_1$ are the on-site fermion parton flavors corresponding to $S_z = -1, 0, 1$.

This could be converted into a MPS by treating it as a general Pfaffian and then applying the techniques in Sec. III B. In models such as this, though, where the mean-field Hamiltonian in the parton basis has a tensor sum structure where one or more of the Hilbert subspaces can be treated with a simpler mean field (i.e., with a SD or BdG ground state) it makes computational sense to obtain the MPS representation in each sector and then "glue" the two MPS together; we exemplify this approach here.

Introducing a Nambu spinor, in the k basis the Hamiltonian is block-diagonal,

$$\begin{aligned} H^k_{\mathrm{mf}} = &\frac{1}{2}\begin{bmatrix} c^\dagger_{k,1} & c_{-k,-1} & c^\dagger_{k,0} & c_{-k,0} \end{bmatrix} \\ &\times \begin{bmatrix} \chi_k & \Delta_k & 0 & 0 \\ \Delta^*_k & -\chi_k & 0 & 0 \\ 0 & 0 & \chi_k & -\Delta_k \\ 0 & 0 & -\Delta^*_k & -\chi_k \end{bmatrix} \begin{bmatrix} c_{k,1} \\ c^\dagger_{-k,-1} \\ c_{k,0} \\ c^\dagger_{-k,0} \end{bmatrix}. \end{aligned} \tag{38}$$

The one-body Hamiltonian is a tensor sum of BdG-like Hamiltonian H_{BdG} and a p-wave Hamiltonian H_p. The mean-field ground state is (we consider antiperiodic boundary conditions and an even number of sites)

$$\begin{aligned} |\Psi_{\mathrm{GS}}\rangle = &\Pi_{0<k<2\pi}(u_k + v_k c^\dagger_{k,1} c^\dagger_{-k,-1}) \\ &\times \Pi_{0<q<\pi}(u_q - v_q c^\dagger_{q,0} c^\dagger_{-q,0})\,|0\rangle\,, \end{aligned} \tag{39}$$

where u_k and v_k are given in terms of the parameters of the Hamiltonian.

By performing a particle-hole transformation in the $S_z = \{\uparrow, \downarrow\}$ sector (see Sec. III A) and the Pfaffian artificial extension in the $S_z = 0$ sector (see Sec. III B),

$$\begin{aligned} f^\dagger_{1,k} &= c^\dagger_{k,1}, \\ f^\dagger_{2,k} &= c_{-k,-1}, \\ f^\dagger_{3,k} &= c^\dagger_{k,0}, \\ f^\dagger_{4,k} &= c_{-k,0}, \end{aligned} \tag{40}$$

where $\{f_{k,\alpha}, f_{q,\beta}\} = \delta_{\alpha\beta}\delta_{kq}$, giving us

$$\begin{aligned} \left|\Psi^{\mathrm{ext}}_{\mathrm{GS}}\right\rangle = &\Pi_k(u_k f^\dagger_{k,2} + v_k f^\dagger_{k,1}) \\ &\times \Pi_{0<q<\Pi}(u_q f^\dagger_{q,4} - v_q f^\dagger_{k,3})\,|\mathrm{vac}\rangle\,, \end{aligned} \tag{41}$$

with $|\mathrm{vac}\rangle = \Pi_{0<k<2\pi} c_{k\downarrow}\,|0\rangle\,\Pi_{0<q<\pi} c_{k,0}\,|0\rangle$. Since $|\Psi^{\mathrm{ext}}_{\mathrm{GS}}\rangle$ is a Slater determinant, we can obtain the MPS representation using the methods in Sec. II. We now "undo" the transformation (see again Secs. III A and III B) and write the MPS in the following form,

$$\begin{aligned} |\mathrm{MPS}\rangle = &\sum_{\{i\}} (C^{[1_\uparrow]i_{1\uparrow}} C^{[1_\downarrow]i_{1\downarrow}} C^{[1,\rightarrow]i_{1,\rightarrow}}) \\ &\times \cdots (C^{[N_\uparrow]i_{N\uparrow}} C^{[N_\downarrow]i_{N\downarrow}} C^{[N,\rightarrow]i_{N\rightarrow}}) \\ &\times |(i_{1_\uparrow} i_{1_\downarrow} i_{1_\rightarrow}) \cdots (i_{N_\uparrow} i_{N_\downarrow} i_{N_\rightarrow})\rangle\,, \end{aligned} \tag{42}$$

where $i_{n,\alpha} \in \{0, 1\}$ indicates the absence/presence of a particle of type α on site n.

To obtain the MPS with on-site tensors $A^{[n]\sigma_n}$, $\sigma_n \in \{\uparrow, \downarrow, \rightarrow, \uparrow\rightarrow, \downarrow\rightarrow, \uparrow\downarrow, \uparrow\downarrow\rightarrow\}$, we "glue" together appropriate

sectors. For example,

$$A^{[n]\uparrow} = C^{[n\uparrow]1} C^{[n\downarrow]0} C^{[n\rightarrow]0}, \tag{43}$$

and the Gutzwiller projection is realized by summing *only* over the one-particle per site physical indices $\sigma_n \in \{\uparrow, \downarrow, \rightarrow\}$:

$$P_{\mathrm{G}} |\Psi_{\mathrm{GS}}\rangle = \sum_{\sigma_n \in \{\uparrow,\downarrow,\rightarrow\}} A^{[1]\sigma_1} \cdots A^{[N]\sigma_N} |\sigma_1 \cdots \sigma_N\rangle . \tag{44}$$

B. iMPS orthogonalization

In this section, we will discuss orthogonalizing our iMPS states. This includes a brief overview of the standard iMPS orthogonalization as well as a detailed description of how we address the degeneracies that appear when Gutzwiller projecting slave-fermion mean-field states onto degenerate ground-state manifolds.

The orthogonalization procedure for a typical iMPS is standard (see Ref. [29] and SM 6 [12] for an intuitive derivation and for more details). The method relies on obtaining the leading right/left eigenvectors of the transfer matrix operator $E = \sum_\sigma A^\sigma \otimes A^{\sigma *}$ where σ runs over the on-site physical index. E admits the following decomposition,

$$E = \sum_i \lambda_i |R\rangle_i \langle L|_i , \tag{45}$$

where $|L\rangle_i$ and $|R\rangle_i$ are left/right eigenvectors of E and $\langle L_i|R_i\rangle = 0$ for λ_i nondegenerate. In the infinite limit only the leading left/right eigenvectors of E survive. If the dominant eigenvalue is nondegenerate, the transfer matrix is given by

$$\lim_{N\to\infty} E^N = |R\rangle \langle L| , \tag{46}$$

where $|R(L)\rangle$ are by definition the eigenvectors corresponding to the dominant eigenvalue. Thus, the dominant left and right eigenvectors correspond to a pure state. The implicitly restarted Arnoldi method can be efficiently used for this purpose by noting that $(\sum_\sigma A^\sigma \otimes A^{\sigma *})\mathrm{vec}(v) = \sum_\sigma \mathrm{vec}(A^{\sigma *} v A^T)$, where the $\mathrm{vec}(v)$ operation takes the square matrix v and stacks the columns together. The entanglement spectrum and observables are then easily obtained.

When the leading eigenvalues of the transfer matrix are degenerate in magnitude,

$$\lim_{N\to\infty} E^N = |R_1\rangle \langle L_1| + |R_2\rangle \langle L_2| , \tag{47}$$

E^N is in mixed form. In general the output of the Arnoldi method gives $\langle L_i|R_i\rangle \neq 0$. Thus, additional steps are required to obtain the canonical form of the iMPS. The degeneracy of the leading eigenvalues signals the presence of degenerate states. This is indeed what happens for the twofold degenerate dimer phase and the fourfold degenerate Haldane phase (in the thermodynamic limit). In order to access all the states in the ground-state manifold, we need to obtain the proper set of pure iMPS states. The transfer matrix of a pure iMPS has unique left/right leading eigenvectors.

Here, we consider the case of twofold degeneracy present in the dimer phase states (other states and higher degeneracies can be dealt with using a similar procedure). For a twofold degenerate iMPS, we need to find two pure iMPS generated by bulk tensors A_1 and A_2. Any iMPS within the degenerate manifold is then able to be written as a linear superposition

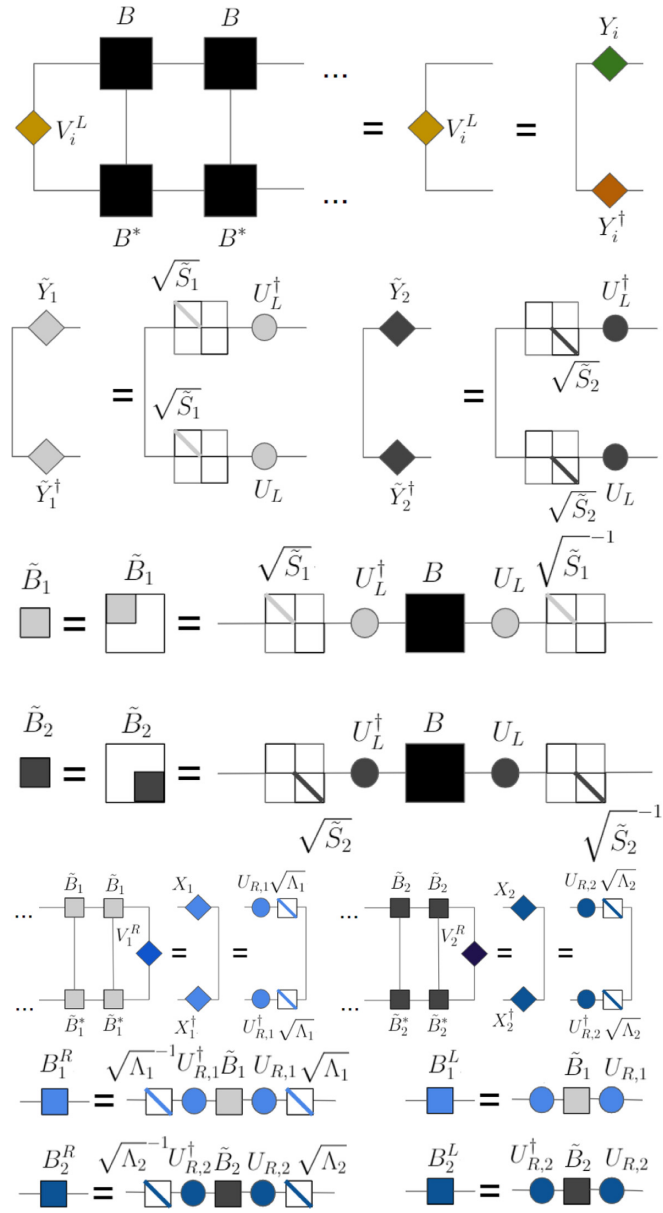

FIG. 7. Illustration of decomposition of a mixed transfer matrix into pure components. In step 1 (first line), we find the dominant left eigenvector of the transfer matrix; In step 4 (second line), we find U_L and $\tilde{S}_1$ and $\tilde{S}_2$. In step 5 (third, fourth, and fifth lines), we form two new tensors $\tilde{B}_i$ and find their right leading eigenvectors. In step 6 (other lines), we find the entanglement spectrum $\sqrt{\Lambda_i}$ and the right/left canonical matrices B_i^R and B_i^L, corresponding to the two pure states.

of these pure states, $|\psi_B\rangle = \alpha_1 |\psi(A_1)\rangle + \alpha_2 |\psi(A_2)\rangle$, where the notation $|\psi(B)\rangle$ indicates the iMPS generated by bulk tensor B. Note that the entanglement spectrum of the reduced density matrix $\rho_B = |\alpha_1|^2 \rho_{A_1} + |\alpha_2|^2 \rho_{A_2}$ is given by the combined spectra of $\alpha_1 \rho_1$ and $\alpha_2 \rho_2$.

To generate these pure iMPS, we start from a noncanonical bulk tensor A iMPS with a single-site unit cell (typically generated by projection). In the case of the dimer phase, this bulk tensor has two leading right (respectively left) eigenvectors, v_1 and v_2, with equal magnitude eigenvalues $|\eta_1| = |\eta_2|$, but different signs (i.e., $\eta_1 = -\eta_2$).

TABLE I. Comparison of energies per site between the exact ground state (iTEBD/DMRG), variational Monte Carlo (VMC), and the fMPS and iMPS generated from the projected slave-fermion states. fMPS are computed with $N = 64$ or $N = 96$ and $10^{-4} \leqslant \epsilon \leqslant 3 \times 10^{-4}$. The bulk tensors used in iMPS have bond dimension $D \approx 1000$. Column headings correspond to (J, K).

	$(1,1)_{\mathrm{ULS}}$	$(1,\frac{1}{3})_{\mathrm{AKLT}}$	$(1,0)_{\mathrm{Heisenberg}}$	$(1,-1)_{\mathrm{TB}}$	$(1,-2)$	$(1,-3)$	$(0,-1)$	$(-1,-3)$	$(-1,-2)$
iTEBD [17]	0.2971	$-\frac{2}{3}$	−1.4015	−4	−6.7531	−9.5330	−2.7969	−7.3518	−4.5939
DMRG	0.2978	$-\frac{2}{3}$	−1.4015	−3.9999	−6.7526	−9.5314	−2.7969	−7.3516	−4.5939
VMC [17]	0.2997	$-\frac{2}{3}$	−1.4001	−3.9917	−6.7372	−9.5103	−2.7953	−7.2901	−4.4946
	±0.0004	$\pm 7 \times 10^{-15}$	±0.0004	±0.0012	±0.0023	±0.0034	±0.0005	±0.0038	±0.0028
fMPS	0.2995	$-\frac{2}{3}$	−1.3999	−3.9895	−6.7369	−9.5073	−2.7948	−7.2877	−4.4935
iMPS		$-\frac{2}{3}$	−1.3999		−6.7368	−9.5071	−2.7947	−7.2877	−4.4934
χ	1	1	1	1	1	1	0	0	0
Δ	0	$\frac{3}{2}$	0.98	1.11	1.15	1.79	1	1	1
λ	1	0	1.78	2.00	2.07	2.22	0.14	0.21	0.12

According to Theorem 5 in Ref. [30] and Theorem 11 in Ref. [31], there is a unitary that transforms each of the matrices $B^{\sigma\sigma'} = A^{\sigma}A^{\sigma'}$ into block-diagonal form, with two blocks; the two blocks are the two-site uniform tensors corresponding to the two pure states.

Based on the mathematical theorems in Refs. [30,31], we use the following procedure to compute the pure states (see Fig. 7):

(1) Start with the $D \times D$ (D is the bond dimension of the bulk tensors A) left leading eigenvectors (with the same eigenvalue), V_1^L and V_2^L, of the completely positive map E^2, i.e., $\sum_{\sigma,\sigma'} B^{\dagger\sigma\sigma'} V_i^L B^{\sigma'} = V_i^L$.

(2) V_i^L are transformed into Hermitian matrices: $V_i^L := 1/2[V_i^L + (V_i^L)^\dagger]$; this is possible because if V_i^L is an eigenvector of E^2, then $(V_i^L)^\dagger$ is also an eigenvector and so their sum is Hermitian. If $V_i^L = U_i D_i U_i^\dagger$, then we can write $V_i^L = Y_i^\dagger Y_i$ with $Y_i = \sqrt{D_i} U_i^\dagger$.

(3) Diagonalize V_1^L and V_2^L together; this can be done since $[V_1^L, V_2^L] = 0$ so that $U^\dagger V_i^L U = S_i$, with S_i being a diagonal matrix.

(4) Form two linear combinations $\tilde{V}_i^L = V_1^L - \alpha_i V_2^L$ where α_i is one of the two nonzero values obtained by the elementwise division of S_1 and S_2. Then $U_L^\dagger \tilde{V}_1^L U_L$ will be a diagonal matrix $\tilde{S}_1$ with entries $(\tilde{d}_1^1, \tilde{d}_1^2, \ldots, \tilde{d}_1^p, 0, 0, \ldots, 0)$ and $U_L^\dagger \tilde{V}_2^L U_L$ a diagonal matrix $\tilde{S}_2$ with entries $(0, 0, \ldots, 0, \tilde{d}_2^{D-k}, \tilde{d}_2^{D-k-1}, \ldots, \tilde{d}_2^D,)$ and $D - k \geqslant p$; in fact, it will almost always be the case that $D - k > p$, since the bond dimension of the canonical bulk tensor decreases after projection; this decomposition is guaranteed by Theorem 5 in Ref. [30].

(5) Form two new two-site bulk tensors $\tilde{B}_i = \sqrt{\tilde{S}_i} U_L^\dagger B U_L \sqrt{\tilde{S}_i}^{-1}$ and obtain their transfer matrix right-leading eigenvectors; they will each have a unique leading Hermitian semipositive definite diagonal eigenvector, $V_i^R = U_{R,i} \Lambda_i (U_{R,i})^\dagger$; we can write $V_i^R = X_i X_i^\dagger$ with $X_i = U_{R,i}\sqrt{\Lambda}$; then $\sqrt{\Lambda_i}$ is the entanglement spectrum of the corresponding pure state.

(6) $B_i^R = \sqrt{\Lambda_i}^{-1} (U_{R,i})^\dagger \tilde{B}_i U_{R,i} \sqrt{\Lambda_i}$ are the right canonical tensors and $B_i^L = (U_{R,i})^\dagger \tilde{B}_i U_{R,i}$ are the left canonical tensors; since $B_i^L \sqrt{\Lambda_i} = \sqrt{\Lambda_i} B_i^R$ the uniform two-site translationally invariant bulk tensors can be written as $A_i = \sqrt{\sqrt{\Lambda_i}} B_i^R \sqrt{\sqrt{\Lambda_i}}^{-1} = \sqrt{\sqrt{\Lambda_i}}^{-1} B_i^L \sqrt{\sqrt{\Lambda_i}}$.

C. Energy of BLBQ slave-fermion wave functions

We compute both the MPS and iMPS (except at the critical points) for the variational Gutzwiller projected wave functions corresponding (as found in Ref. [17] by minimizing the variational energy) to the points in Fig. 6. We directly compare the energy for all of these points (see Table I) and find that the energies are all within the error bars reported for the VMC calculation [17].

D. Entanglement spectra of BLBQ slave-fermion wave functions

1. Dimer phase

In this section, we will consider entanglement spectra of the dimerized phase of the BLBQ model. The ground state of the dimerized phase is twofold degenerate depending on whether the dimer covering spans even or odd bonds; the entanglement spectra also depends on whether the entanglement cut is made through or between dimers. For the fMPS, we can obtain both the even and odd cut entanglement spectra of the dimerized states by choosing two consecutive cuts whereas for the iMPS we use the procedure described in Sec. IV B to find the two pure states which correspond respectively to the even and odd cuts.

We start by considering a generic slave-fermion point in the BLBQ model; see Fig. 8 for the entanglement spectrum (ES). The iMPS and fMPS slave-fermion point agrees well both with each other and the exact ES from DMRG.

The low-lying level of the entanglement spectrum cycles between a singlet and a triplet as we move the location of the entanglement cut within the chain. This is indicative of translation invariance breaking and the dimerized structure of the ground state: Namely the low-level singlet is associated with a cut between dimers, whereas the low-level triplet is associated with a cut inside dimers.

We can also further understand the higher states in the entanglement spectra. A generic point in the dimer phase of the BLBQ model is SU(2) symmetric. Consequently, the entanglement levels transform under SU(2) representation and

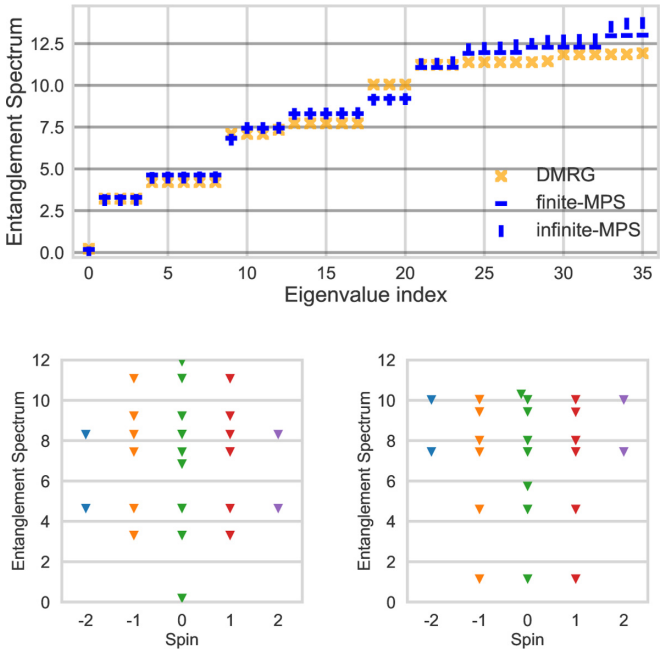

FIG. 8. Entanglement spectra of the projected mean-field state from iMPS and fMPS at $(J, K) = (1, -2)$ showing (a) the comparison with DMRG between dimers, and the fMPS spin-resolved ES (b) between dimers and (c) within dimers. Note that the single and triple degeneracies seen in (b) and (c) are the expected low-level structures seen in a pure VBS state. The lowest three entanglement levels of (b) are representations of SU(2): singlet, triplet, and quintet.

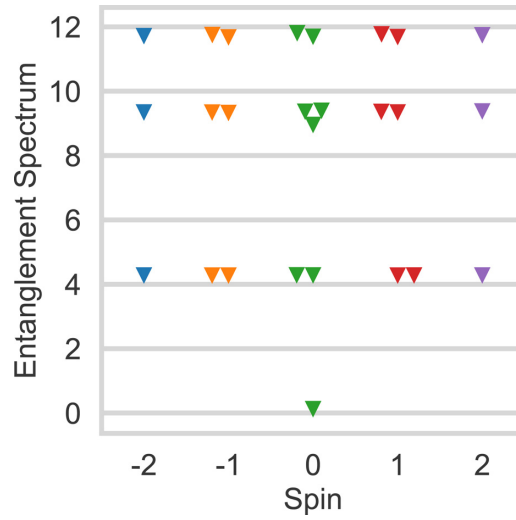

FIG. 9. Spin-resolved entanglement spectrum (between dimers) for the $(J, K) = (0, -1)$ variational point generated from fMPS. The SU(3) symmetry forces the $S = 1$ and $S = 2$ into a degenerate octet.

therefore we expect that degeneracies should go as the dimension of SU(2) representations (i.e., $2n + 1$ for non-negative integer n); this can be seen in the multiplet structure of both the entanglement spectra in Fig. 8 (bottom left), where the lowest three degeneracies between dimers form the singlet ($S = 0$), triplet ($S = 1$), and quintuplet ($S = 2$).

Beyond considering a generic point within the dimer phase, we now consider the exactly solvable point where $(J, K) = (0, -1)$ [the so-called Klümper-Barber-Batchelor (KBB) point [32,33]], which is invariant under a larger symmetry group, SU(3) [as opposed to SU(2)]. This larger symmetry group forces the triplet and quintet to form an octet [the adjoint representation of SU(3)]. Variationally, the vanishing of the hopping parameter in the slave-fermion mean-field Hamiltonian forces this larger symmetry group at the level of the variational Gutzwiller projected wave function. See Fig. 9.

The points $(J, K) = (-1, -2)$ and $(J, K) = (-1, -3)$ which are found at a variational minima with $t = 0$ in the parent Hamiltonian by Ref. [17] also have SU(3) symmetry. This symmetry is not present in the true DMRG ground state which transforms only under SU(2) symmetry; therefore, a better agreement is obtained by perturbing slightly away from this point (see SM 7 [12] for entanglement spectrum data of the slightly perturbed points).

2. *Haldane phase*

In this section we compute the entanglement spectra of the AKLT and Heisenberg points belonging to the Haldane phase of BLBQ. The slave-fermion mean field for this model has a fourfold degeneracy at the Fermi level that allows for choosing six orthogonal preprojected mean-field states (at half filling). Projecting each of these states generates (postprojection) a space of MPS which span four degenerate ground states which correspond to the representations of the sum of the two fractionalized $S = 1/2$ edge modes of the Haldane phase.

Here, we start by considering the AKLT point which has an exact analytic solution. The AKLT point $(J, K) = (1, 1/3)$ is exactly mapped under the above slave-fermion projective construction to $(\chi, \delta, \mu) = (1, 3/2, 0)$. To find the AKLT state which (for example) has the edge modes $\uparrow\downarrow$ we can either search in the fourfold projected degenerate space or choose the correct orbitals at the Fermi-level preprojection. We find the entanglement spectra for each of the four fMPS which correspond to $\downarrow\downarrow$, $\downarrow\uparrow$, $\uparrow\downarrow$, $\uparrow\uparrow$ edge spin configurations is equal to $\ln(2)$.

For the iMPS, unlike the dimer phase, where there was twofold degeneracy in the leading eigenvalues of the transfer matrix operator for points in the Haldane phase, we find fourfold degeneracy. We obtain two-negative and two-positive (equal in magnitude) leading eigenvalues. Taking the space spanned by the two eigenvectors with positive eigenvalues, we apply the iMPS orthogonalization procedure from Sec. IV B. From this process, for the AKLT slave-fermion point we find after orthonormalization the iMPS

$$A^0 = \begin{pmatrix} -1 & 0 \\ 0 & 1 \end{pmatrix},$$
$$A^{\downarrow} = \sqrt{2}\begin{pmatrix} 0 & -e^{-i\theta} \\ 0 & 0 \end{pmatrix}, \tag{48}$$
$$A^{\uparrow} = \sqrt{2}\begin{pmatrix} 0 & 0 \\ e^{i\theta} & 0 \end{pmatrix},$$

associated with two pure states (i.e., $|\uparrow\downarrow\rangle$ and $|\downarrow\uparrow\rangle$ of the edge modes). In SM 8 [12], we also obtain the iMPS representation of the $S = 1/2$ VBS ground state of the Majumdar-Ghosh (MG) chain [34,35].

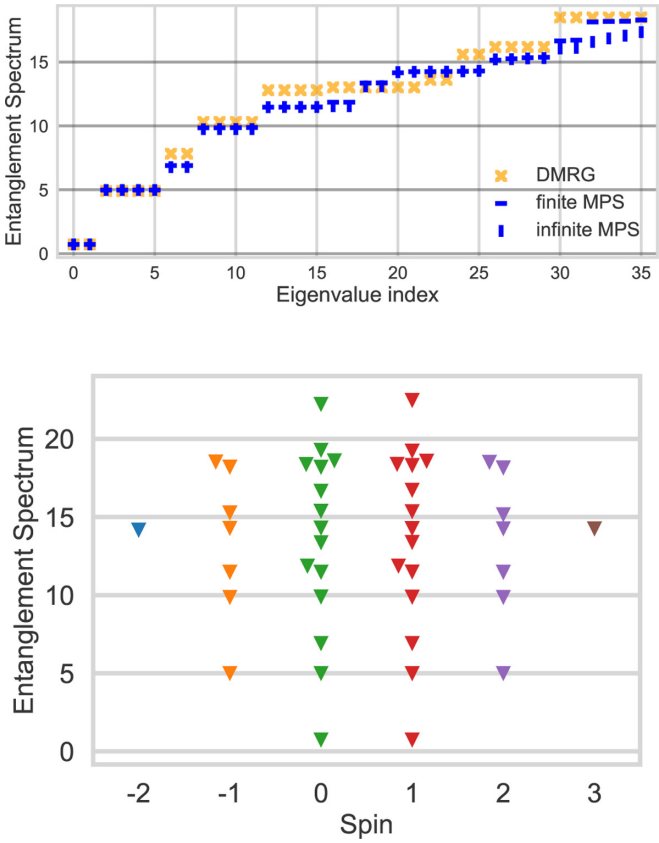

FIG. 10. Top: Comparison of entanglement spectrum obtained from fMPS, iMPS, and DMRG at the $(J, K) = (1, 0)$ Heisenberg point. Bottom: Spin-resolved entanglement spectrum from fMPS at the $(J, K) = (1, 0)$ Heisenberg point in the $(S = 1, S_z = 1)$ sector.

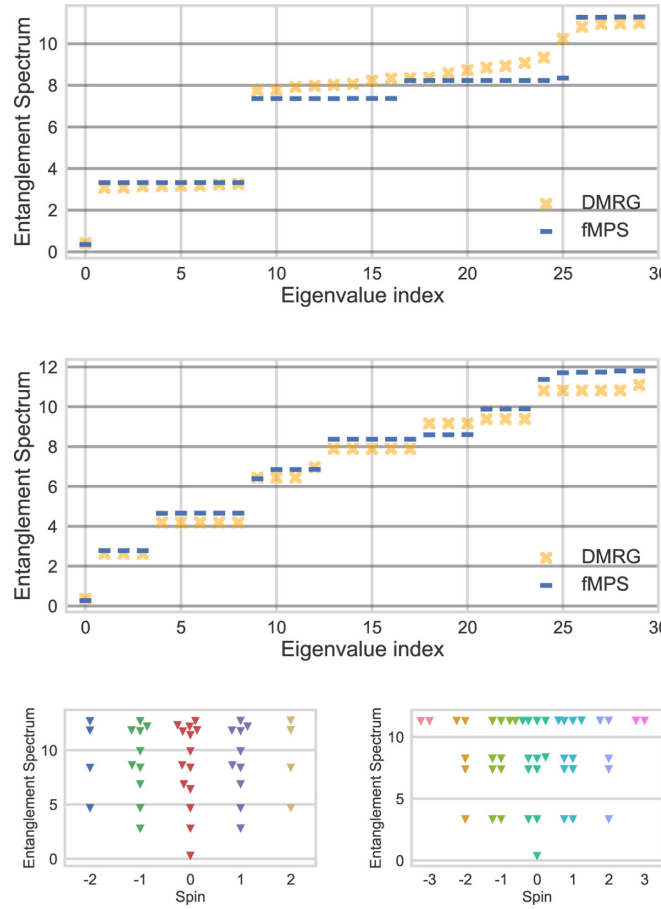

FIG. 11. (a) Comparison of entanglement spectra at the ULS point for fMPS and DMRG. (b) Comparison of entanglement spectra at the TB point for fMPS and DMRG. (c) Spin-resolved entanglement spectrum for the (left) TB point and (right) ULS point.

In Fig. 10 we also present the entanglement spectrum of the Heisenberg point $(J, K) = (1, 0)$ obtained using both fMPS and iMPS. We see that the lower levels match well the entanglement spectrum levels obtained from DMRG of the true Heisenberg ground state. Discrepancies occur naturally higher up in the spectrum as the variational wave function is not the *exact* ground state. However, the entanglement spectrum of the variational ground state (qualitatively) captures the symmetries and degeneracies of the *true* entanglement spectrum. Note the fact that every level has even degeneracy comes from the topological nature of the phase. Moreover, notice that the lowest parts of the entanglement spectra match the AKLT state in the same sector.

3. *Critical points*

We compute the two critical points at $(J, K) = (1, -1)$ [the Takhtajan-Babujian (TB) point [36,37]] and at $(J, K) = (1, 1)$ [the Uimin-Lai-Sutherland (ULS) [38–40]]; they are gapless and hence we analyze them only in the framework of our fMPS method. The TB ground state is unique; the associated effective conformal field theory is $\mathrm{SU}(2)|_{k=2}$.

The ULS ground state is also unique. However, it has an enlarged SU(3) symmetry group; the associated effective conformal field theory is $\mathrm{SU}(3)|_{k=1}$. In particular it can be mapped to the SU(3) nearest-neighbor Heisenberg model [41]. This enforces an equal number of "quark" particle constraints (and hence a global equal number of spins $1, -1, 0$). At the mean-field level, the pairing parameter vanishes since $J - K = 0$. The Hamiltonian is then a tensor sum of 3 identical hopping Hamiltonians acting independently on the fermions of flavor "up," "down," and "zero." The particle number constraint of c_1, c_{-1}, c_0 is naturally enforced at the mean-field level if the number of sites N is a multiple of 3.

The SU(3) symmetry of the ULS point is reflected in the degeneracies of the entanglement spectrum where the $S = 1$ and $S = 2$ levels combine together to form SU(3) octets as can be seen in Fig. 11. For the TB point the $S = 1$ and $S = 2$ entanglement levels remain separated.

The central charge of $\mathrm{SU}(N)|_k$ conformal field theories (CFTs) is given by $c = k(N^2 - 1)/(N + k)$. Hence, analytically $c = 1.5$ for the TB point and $c = 2$ for ULS. Calabrese and Cardy [42] obtained the following expression for the entanglement entropy scaling for a 1D critical gapless point of finite size L with open-boundary conditions and partition size x,

$$S(x, L) = \frac{c}{6} \ln \frac{2L}{\pi} \sin\left(\frac{\pi x}{L}\right) + \ln g + s_1/2, \qquad (49)$$

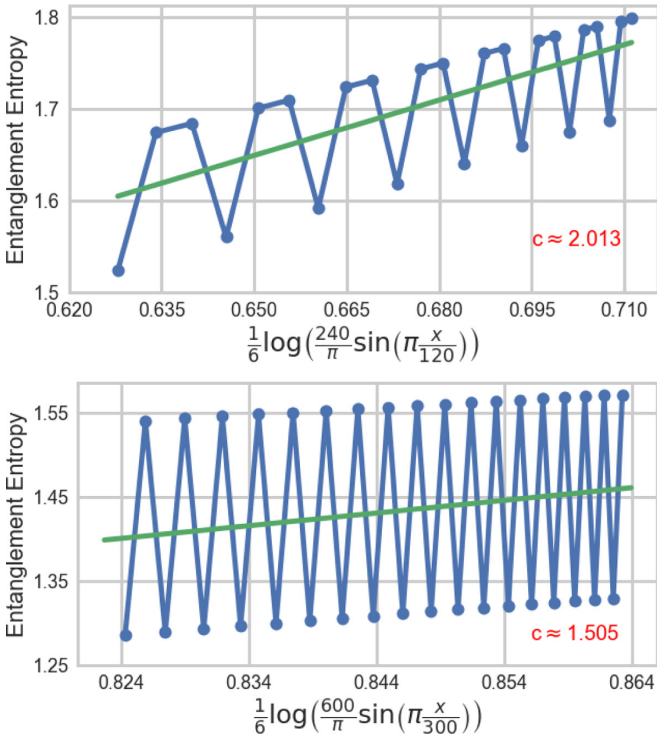

FIG. 12. The von Neumann entanglement entropy scaling of the slave-fermion wave functions describing the ULS critical point (top) for a system of size $L = 120$ and the TB (bottom) critical point for a system of size $L = 300$ computed with fMPS. Shown also is the central charge obtained from least squares fitting.

where $\ln g$ is a boundary entropy term and $S(x, L)$ is the von Neumann entanglement entropy.

It was found in Ref. [43] that there is an additional alternating term in $S(x, L)$ which decays away from the boundaries. In Fig. 12 we plot the entanglement entropy against $\frac{c}{6}\ln\frac{2L}{\pi}\sin(\frac{\pi x}{L})$ for both TB and ULS models. We work on a system of size $L = 300$ and plot the region $x \in [75, 110]$ for TB and a system of size $L = 120$ and plot the region $x \in [21, 44]$ for ULS. We picked the lower bounds to be far enough from the boundary and the upper bounds to work in the region of the sine curve with x away from $L/2$ where the curve becomes very flat. For the SU(3) ULS point, when x is a multiple of 3, the highest eigenvalue Schmidt vector contains equal numbers of "quarks" and hence is dominant. For cuts at $x = 3k + 1, 3k + 2$ (for integer k), the Schmidt vectors cannot satisfy the particle conservation constraint and hence the highest eigenvalue Schmidt vectors are degenerate. A similar situation occurs at the SU(2) TB point where the 2-periodicity is easily explained in the dimer picture: For even cuts we cut between dimers, whereas for odd cuts we break dimers and hence split the singlet apart. The alternating term is still significant for the parameters we chose. Hence, it is difficult to reliably extract the central charge. However, we manage to obtain results for central charges at both points which are remarkably close to their theoretical values: 2.013 as compared to 2.0 for the ULS point and 1.505 as compared to 1.5 for the TB point. We overlay the lines obtained from least-squares fitting for both models.

V. DISCUSSION AND FUTURE WORK

We have developed a series of efficient and highly parallel algorithms to obtain the finite and infinite (for gapped states) MPS representation of fermionic mean-field states. Gutzwiller projection is easily implemented by eliminating the doubly occupied and unoccupied physical sectors of the mean-field slave-fermion MPS tensors. We have used these methods to obtain the (i)MPS representation of Gutzwiller projected mean-field states that arise from the variational slave-fermion approach to the $S = 1$ bilinear-biquadratic (BLBQ) quantum spin chain introduced in Ref. [17]. We first verify that the energies we obtain via both finite MPS and infinite MPS (not applicable to the critical points) for the points considered are within the error bars of their VMC calculations [17].

Additionally, we obtain the entanglement spectra at two critical points (ULS and TB) and several generic points in the dimer and Haldane phases of the BLBQ model. We find good qualitative (and quantitative) agreement with results obtained directly from DMRG. We briefly discuss the salient structural features of the entanglement spectrum in all the phases (but see Ref. [41] for a more detailed analysis). Extracting the central charges of the conformal field theories describing the two gapless critical points from a numerical computation of the entanglement spectrum on finite open-boundary systems is made difficult by a slowly decaying oscillatory term in the entanglement entropy. However, we do obtain very good agreement for the central charge at both the ULS and TB point: 2.013 as compared to the exact analytical value of 2.0 for the ULS point and 1.505 as compared to the exact analytical value of 1.5 for TB.

We also introduce an algorithmic procedure that orthogonalizes an iMPS by breaking it down into its pure states. This is essential when dealing with degenerate ground states that appear upon Gutzwiller projection as is the case with points in the dimer phase of the BLBQ model. Having obtained the pure states, we can compute the entanglement spectrum for any state in the ground-state manifold. We check that the entanglement spectrum obtained from iMPS matches the one we obtain from the finite MPS procedure. Discrepancies naturally appear as we approach values close to the thresholds used to generate the finite MPS and infinite MPS.

The methods can be easily adapted to the study of systems on 2D ladders (infinite in length but with finite width). The iMPS unit cell is now formed by the tensors sitting on the width of the cylinder. We will explore the applications of Gutzwiller projected variational wave functions to the study of 2D quantum spin liquids in future publications. This method may also be applicable to topological states such as quantum Hall and fractional Chern insulators that are represented as products of mean-field wave functions.

ACKNOWLEDGMENTS

B.K.C. acknowledges support from the Department of Energy Grant No. DOE de-sc0020165. This project is part of the Blue Waters sustained petascale computing project, which is supported by the National Science Foundation (Awards No. OCI-0725070 and No. ACI-1238993) and the State of Illinois. Blue Waters is a joint effort of the University of

Illinois at Urbana-Champaign and its National Center for Supercomputing Applications. G.K.-L.C. was supported by the US National Science Foundation via Grant No. 1839204. G.K.-L.C. also acknowledges support from the Simons Foundation via the Investigator Award and the Many-Electron Collaboration.

[1] A. J. Leggett, *Quantum Liquids: Bose Condensation and Cooper Pairing in Condensed-Matter Systems* (Oxford University Press, Oxford, U.K., 2006).

[2] N. Read and D. Green, Paired states of fermions in two dimensions with breaking of parity and time-reversal symmetries and the fractional quantum Hall effect, Phys. Rev. B **61**, 10267 (2000).

[3] M. T. Fishman and S. R. White, Compression of correlation matrices and an efficient method for forming matrix product states of fermionic Gaussian states, Phys. Rev. B **92**, 075132 (2015).

[4] Y.-H. Wu, L. Wang, and H.-H. Tu, Tensor Network Representations of Parton Wave Functions, Phys. Rev. Lett. **124**, 246401 (2020).

[5] H.-K. Jin, H.-H. Tu, and Y. Zhou, Efficient tensor network representation for Gutzwiller projected states of paired fermions, Phys. Rev. B **101**, 165135 (2020).

[6] N. Schuch and B. Bauer, Matrix product state algorithms for Gaussian fermionic states, Phys. Rev. B **100**, 245121 (2019).

[7] U. Schollwöck, The density-matrix renormalization group in the age of matrix product states, Ann. Phys. **326**, 96 (2011).

[8] S.-A. Cheong and C. L. Henley, Many-body density matrices for free fermions, Phys. Rev. B **69**, 075111 (2004).

[9] I. Klich, Lower entropy bounds and particle number fluctuations in a Fermi sea, J. Phys. A: Math. Gen. **39**, L85 (2006).

[10] G. Knizia and G. K.-L. Chan, Density Matrix Embedding: A Simple Alternative to Dynamical Mean-Field Theory, Phys. Rev. Lett. **109**, 186404 (2012).

[11] I. Peschel, Special review: Entanglement in solvable many-particle models, Braz. J. Phys. **42**, 267 (2012).

[12] See Supplemental Material at http://link.aps.org/supplemental/10.1103/PhysRevB.103.125161 for more details regarding the Schmidt decomposition of Slater determinants, the mathematical expression of the boundary tensors, entanglement spectrum data in the context of the SSH model, a mathematical derivation, how we deal with gapless boundary modes in the context of the iMPS procedure, an intuitive derivation, entanglement spectrum data of the slightly perturbed points, and derivations and numerical data.

[13] D. A. Harville, *Matrix Algebra from a Statistician's Perspective* (Springer, New York, 1997).

[14] W. P. Su, J. R. Schrieffer, and A. J. Heeger, Solitons in Polyacetylene, Phys. Rev. Lett. **42**, 1698 (1979).

[15] S. Ripka, J. Blaizot, and G. Ripka, *Quantum Theory of Finite Systems* (MIT Press, Cambridge, MA, 1986).

[16] A. Y. Kitaev, Unpaired Majorana fermions in quantum wires, Phys. Usp. **44**, 131 (2001).

[17] Z.-X. Liu, Y. Zhou, H.-H. Tu, X.-G. Wen, and T.-K. Ng, Gutzwiller projected wave functions in the fermionic theory of $S = 1$ spin chains, Phys. Rev. B **85**, 195144 (2012).

[18] F. D. M. Haldane, Continuum dynamics of the 1-D Heisenberg antiferromagnet: Identification with the O(3) nonlinear sigma model, Phys. Lett. A **93**, 464 (1983).

[19] I. Affleck, T. Kennedy, E. H. Lieb, and H. Tasaki, Valence bond ground states in isotropic quantum antiferromagnets, in *Condensed Matter Physics and Exactly Soluble Models* (Springer, Berlin, 1988), pp. 253–304.

[20] Z.-C. Gu and X.-G. Wen, Tensor-entanglement-filtering renormalization approach and symmetry-protected topological order, Phys. Rev. B **80**, 155131 (2009).

[21] F. Pollmann, E. Berg, A. M. Turner, and M. Oshikawa, Symmetry protection of topological phases in one-dimensional quantum spin systems, Phys. Rev. B **85**, 075125 (2012).

[22] A. M. Turner, F. Pollmann, and E. Berg, Topological phases of one-dimensional fermions: An entanglement point of view, Phys. Rev. B **83**, 075102 (2011).

[23] F. Pollmann, A. M. Turner, E. Berg, and M. Oshikawa, Entanglement spectrum of a topological phase in one dimension, Phys. Rev. B **81**, 064439 (2010).

[24] H. Li and F. D. M. Haldane, Entanglement Spectrum as a Generalization of Entanglement Entropy: Identification of Topological Order in Non-Abelian Fractional Quantum Hall Effect States, Phys. Rev. Lett. **101**, 010504 (2008).

[25] M. Levin and X.-G. Wen, Detecting Topological Order in a Ground State Wave Function, Phys. Rev. Lett. **96**, 110405 (2006).

[26] A. Kitaev and J. Preskill, Topological Entanglement Entropy, Phys. Rev. Lett. **96**, 110404 (2006).

[27] Z.-X. Liu, Y. Zhou, and T.-K. Ng, Fermionic theory for quantum antiferromagnets with spin $S > \frac{1}{2}$, Phys. Rev. B **82**, 144422 (2010).

[28] Z.-X. Liu, Y. Zhou, and T.-K. Ng, Gutzwiller approach for elementary excitations in $S = 1$ antiferromagnetic chains, New J. Phys. **16**, 083031 (2014).

[29] R. Orus and G. Vidal, Infinite time-evolving block decimation algorithm beyond unitary evolution, Phys. Rev. B **78**, 155117 (2008).

[30] D. Perez-Garcia, F. Verstraete, M. M. Wolf, and J. I. Cirac, Matrix product state representations, Quantum Inf. Comput. **7**, 401 (2007).

[31] M. S. Ruiz, Tensor networks in condensed matter, Ph.D. thesis, Technische Universität München, 2011.

[32] A. Klümper, New results for q-state vertex models and the pure biquadratic spin-1 Hamiltonian, Europhys. Lett. **9**, 815 (1989).

[33] M. N. Barber and M. T. Batchelor, Spectrum of the biquadratic spin-1 antiferromagnetic chain, Phys. Rev. B **40**, 4621 (1989).

[34] C. K. Majumdar and D. K. Ghosh, On next-nearest-neighbor interaction in linear chain. I, J. Math. Phys. **10**, 1388 (1969).

[35] V. Karimipour and L. Memarzadeh, Matrix product representations for all valence bond states, Phys. Rev. B **77**, 094416 (2008).

[36] L. Takhtajan, The picture of low-lying excitations in the isotropic Heisenberg chain of arbitrary spins, Phys. Lett. A **87**, 479 (1982).

[37] H. Babujian, Exact solution of the one-dimensional isotropic Heisenberg chain with arbitrary spins S, Phys. Lett. A **90**, 479 (1982).

[38] G. Uimin, One-dimensional problem for $S = 1$ with modified antiferromagnetic Hamiltonian, JETP Lett. **12**, 225 (1970).

[39] C. Lai, Lattice gas with nearest-neighbor interaction in one dimension with arbitrary statistics, J. Math. Phys. **15**, 1675 (1974).

[40] B. Sutherland, Model for a multicomponent quantum system, in *Exactly Solvable Models Of Strongly Correlated Electrons* (World Scientific, Singapore, 1994), pp. 287–297.

[41] R. Thomale, S. Rachel, B. A. Bernevig, and D. P. Arovas, Entanglement analysis of isotropic spin-1 chains, J. Stat. Mech.: Theory Exp. (2015) P07017.

[42] P. Calabrese and J. Cardy, Entanglement entropy and quantum field theory, J. Stat. Mech.: Theory Exp. (2004) P06002.

[43] N. Laflorencie, E. S. Sørensen, M.-S. Chang, and I. Affleck, Boundary Effects in the Critical Scaling of Entanglement Entropy in 1D Systems, Phys. Rev. Lett. **96**, 100603 (2006).